WIMP MASS Determination

Jack Gunion
U.C. Davis

SUSY09, June 4, 2009

Based on:
Cheng,Gunion,Han,Marandella,McElrath (CGHMM) arXiv:0707.0030,
Cheng,Engelhardt,Gunion,Han,McElrath (CEGHM) arXiv:0802.4290,
Cheng, Han (CH) arXiv:0810.5178,
Cheng,Gunion,Han,McElrath (CGHM) arXiv:0905.1344.

Project WIMPMASS webpage: http://particle.physics.ucdavis.edu/hefti/projects/
Assumes input event files in LHE format.

Motivations for an invisible particle below the TeV Scale

1. To solve the Higgs boson mass hierarchy problem there must be new particles below the TeV scale.

2. Sub-TeV new physics avoids precision electroweak constraints most easily if there is a new discrete symmetry that requires that they couple in pairs to the SM particles (especially, the W and Z).

3. The lightest such new particle will then be stable and could explain the observed dark matter in the universe.

4. In many models the correct dark matter density can be obtained and it will have evaded observational contraints (dark matter detection, ...) if this new particle is weakly interacting, $\longrightarrow$ WIMP

   $\Rightarrow$ 2 such particles (call them N) per LHC event that lead to variable and partially balancing missing momentum in each event.

5. Can we determine masses of particles in the chain, especially the N?

As a basic reference, we will often use the mSUGRA SPS1a point with GUT-scale parameters

$$m_0 = 100\ \mathrm{GeV}, m_{1/2} = 250\ \mathrm{GeV}, A_0 = -100\ \mathrm{GeV}, \tan\beta = 10, \mu > 0\,. \quad (1)$$

The decay chain of interest will be

$$\widetilde{q}_L \to q\,\widetilde{\chi}_2^0 \to q\,\ell\,\widetilde{\ell}_R \to q\,\ell\,\bar{\ell}\,\widetilde{\chi}_1^0, \quad (\ell = e, \mu), \quad (2)$$

with the relevant masses being (some variation with program)

$$m_{\widetilde{\chi}_1^0}, m_{\widetilde{\ell}_R}, m_{\widetilde{\chi}_2^0}, m_{\widetilde{u}_L/\widetilde{d}_L} = 97.4, 142.5, 180.3, 564.8/570.8\ \mathrm{GeV}\,. \quad (3)$$

Using lepton spectrum edges and the like yields a good determination of mass differences, but a really precise determination of the overall mass scale is more difficult.

ATLAS studied mass determination using edges. With enough edges, there is sensitivity to the overall mass scale. The results (using the full decay $\widetilde{q}_L$ decay chain above and **ATLFAST**!) summarized in the LHC/LC project (hep-ph/0410364, fhep-ph/0403133 with $L = 300\ \mathrm{fb}^{-1}$) were:

$$\Delta m_{\widetilde{\chi}_1^0} \sim \Delta m_{\widetilde{\chi}_2^0} \sim \Delta m_{\widetilde{\ell}_R} \sim 4.8 - 5\ \mathrm{GeV},$$
$$\Delta m_{\widetilde{q}_L} \sim 9\ \mathrm{GeV}\,, \quad \Delta m_{\widetilde{g}} \sim 8\ \mathrm{GeV}.$$

Can we do better? Can we find *independent* cross-checks?

General Strategy:

- One would like to use pure kinematics to get the absolute masses, *i.e.* not use cross sections, momentum correlations, *etc.*, which are are presumably quite model dependent.

- Use leptons (less smearing, smaller backgrounds) and try to find ways to observe "peaks" as opposed to "edges", the former being more vulnerable to smearing, poor statistics, and backgrounds.

- **Then**, once the masses are known one can input these into the various possible models and much more reliably employ cross sections, correlations and so forth to discriminate between models.

- The focus of the Davis Project **WIMPMASS** is on using the full kinematic information available in an event to get the masses.

Stransverse Mass, M_{T2}: Review

We consider only SUSY-like events with two chains and two Ns.

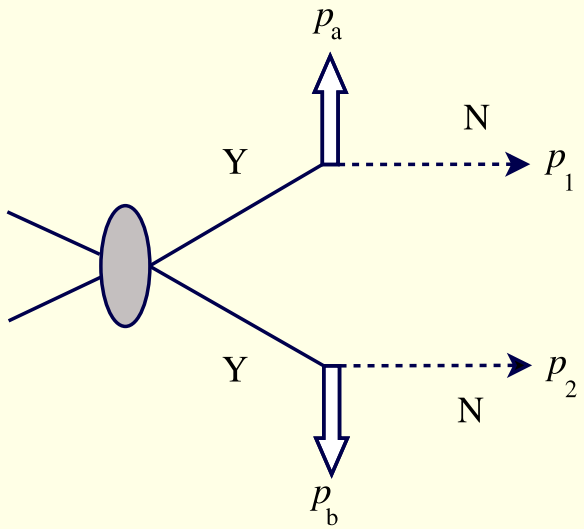

Figure 1: *Construction of M_{T2}. (I discuss only pair production of two chains.)*

1. **Assume a value for N mass, μ_N.**

2. **Consider all partitions of $\not{p}_T = p_T^{(1)} + p_T^{(2)}$.**

$$M_{T2}(\mu_N) \equiv \mathrm{Min}_{\not{p}_T = p_T^{(1)} + p_T^{(2)}} \left[\mathrm{Max} \left\{ M_T(1, a; \mu_N), M_T(2, b; \mu_N) \right\} \right] \quad (4)$$

Basically, The function $M_{T2}(\mu_N)$ is the boundary between the allowed and the forbidden regions in the 2-dimensional $\mu_Y - \mu_N$ mass space constructed from the minimal kinematic constraints of the given event.

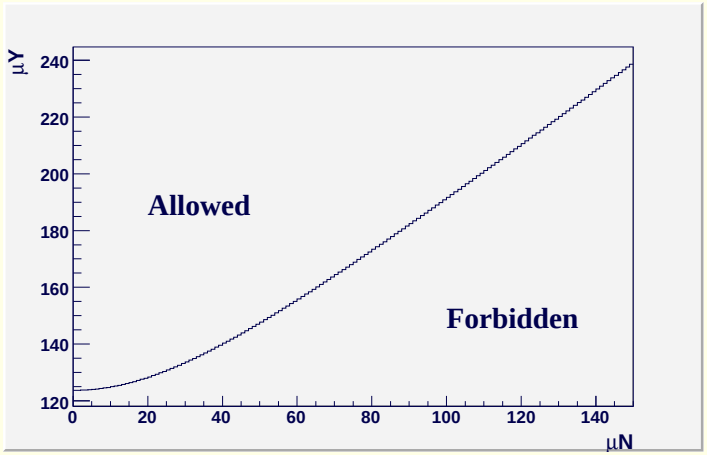

Figure 2: *Allowed regions in $\mu_Y - \mu_N$ mass space are separated by $M_{T2}(\mu_N)$ curve.*

The currently fastest code for computing M_{T2}, based on arXiv:0810.5178, appears on the Project WIMPMASS website.

After accumulating many events, one can assume a value of μ_N and plot the number of events as a function of M_{T2}. The plot will display an upper edge at $M_{T2}^{max}(\mu_N)$.

Crucial to remember: $M_{T2}^{max}(\mu_N)$ gives the correct mother particle mass M_Y for the correct (but unknown) value of $\mu_N = M_N$.

To determine the actual value of M_N, one turns to kinks.

Accumulate many events, and examine $M_{T2}^{max}(\mu_N)$ vs. trial mass μ_N.

If there are 2 or more visible particles per chain aside from the N, $M_{T2}(\mu_N)$ has 2 branches and exhibits a kink at the correct $\mu_N = M_N$ mass value (Cho, et al., arXiv:ls ,0711.4526; see also Barr, Gripaios, Lester, arXiv:0711.4008).

Consider two chains of type $Y \to v_1 X \to v_1 v_2 N$, and compare X off-shell and X on-shell.

X off-shell $\Rightarrow$ good kink; X on-shell $\Rightarrow$ no visible kink.

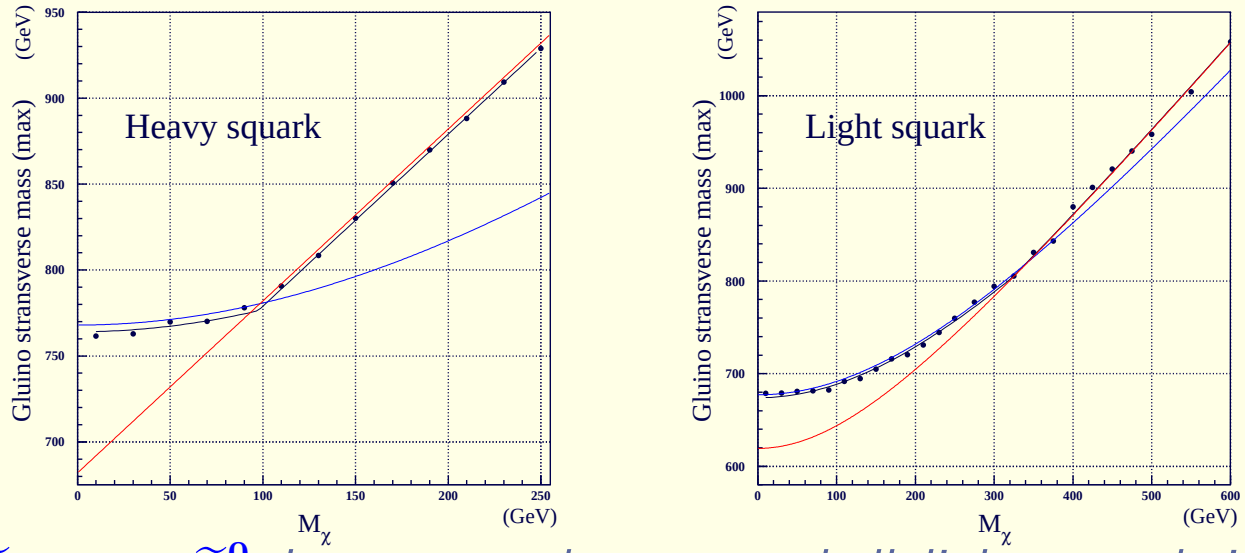

Figure 3: $\widetilde{g} \to qq\widetilde{\chi}_1^0$ *heavy squark vs. on-shell light squark intermediate state. From Cho et al.*

I will focus in this talk on the case of multi-two-body decay chains, for which the M_{T2}^{max} kink is hard to see. This is where technology from the Davis group has its greatest impact. But, also the X^* case can be improved using our event counting game first introduced in CGHMM and then pursued in CEGHM,CH,CGHM.

The on-shell $X = \widetilde{\ell}_R$ case is somewhat different.

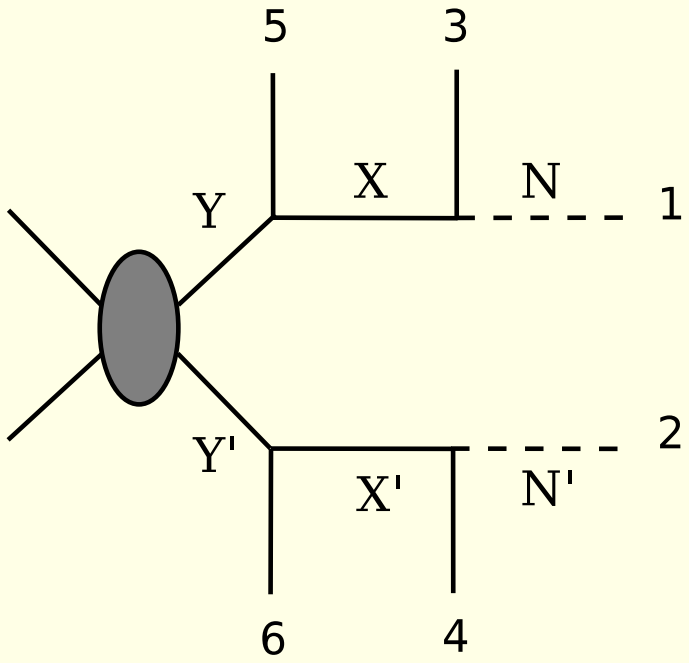

Figure 4: *On-shell topology case.*

- **Davis approach has been to map from kinematic observables to mass space. In this approach, it is useful to define two types of situations:**
  - **Marginal: Each event defines a region in the space of the unknown masses for which the observed visible momenta and missing momentum can be possible.**

    But, no matter how many events, cannot invert kinematic observables to solve for discrete values of the unknown masses in the chains.

    After many events one obtains a well-defined region in the multi-dimensional mass space that is consistent with all events.

    Counting the number of events near the edges of the consistent mass region can allow determination of all masses.

    For two-chain events (the standard situation), if one considers all available information from both chains then the case of two observable particles per chain is a "Marginal" case.
  - **Solvable: The kinematic observables of a finite number of events yields a discrete set of possible values for the unknown chain masses.**

    In the standard two-chain event scenario and considering all information from both chains "solvable" requires that each of the two chains has 3 (or more) visible particles per chain.

Marginal and "Solvable" cases: Basic Constraint Counting

One chain employed, but two chains present.

1. **The "marginal" case is 3 visible particles (or combinations of particles) with 3 on-shell resonances involved and 1 final invisible particle:**

$$Z \to Y v_1 \to X v_2 v_1 \to N v_3 v_2 v_1$$
$$(e.g.\ \widetilde{q}_L \to q\,\widetilde{\chi}_2^0 \to q\,\ell\,\widetilde{\ell}_R \to q\,\ell\,\overline{\ell}\,\widetilde{\chi}_1^0, \quad (\ell = e, \mu)) \tag{5}$$

2. **The first "solvable" case is 4 visible particles with 4 on-shell resonances and the final N.**

$$e.g. \quad \widetilde{g} \to q'\widetilde{q}_L \to q'q\,\widetilde{\chi}_2^0 \to q'q\,\ell\,\widetilde{\ell}_R \to q'q\,\ell\,\overline{\ell}\,\widetilde{\chi}_1^0, \quad (\ell = e, \mu) \tag{6}$$

after n events there are $5 + 4n$ unknowns and $5n$ constraints, implying equality when $n = 5$. So, if there were no combinatoric / resolution issues,

$n = 5$ events would allow you to solve for the 5 masses aside from (very considerable) discrete quartic equation solution ambiguities.

Two (identical) chain examples

1. The "marginal" case here is just two visible particles per chain: $Y \to Xv_1 \to Nv_2v_1$ (e.g. $\widetilde{\chi}_2^0 \to \ell\widetilde{\ell}_R \to \ell\bar{\ell}\,\widetilde{\chi}_1^0$).

   If we assume equal masses on the two chains, then there are 3 unknown masses, including m_N.

   For each event, there are the two 4-momenta of the two final N's, but we know the sum of their transverse momenta from balancing against the visible particle transverse momenta, implying 6 unknown momenta components per event.

   After n events, the number of unknowns is then $3 + 6n$.

   The number of constraints is $6n$ (since we assume on-shell masses on both chains.)

   Thus, no matter how many events, we always have the 3 unknown mass parameters that cannot be absolutely solved for.

Note that by considering both chains, we are at the marginal situation with just 2 visible particles and 2 on-shell resonances plus the 1 final invisible particle, as opposed to the one-chain case where marginality required 3 visible particles, corresponding to 3 on-shell resonances plus 1 invisible particle.

2. The first non-marginal case is clearly 3 visible particles *per chain* ($Z \to Yv_1 \to Xv_2v_1 \to Nv_3v_2v_1$), corresponding to $3+1=4$ unknown masses.

   In this case, after n events we have $4+6n$ unknowns and $8n$ on-shell constraints (recall we have two chains each of which has four mass constraints) implying solution (subject to discrete ambiguities) when $4+6n-8n=0 \Rightarrow n=2$.

   There is a reduction in the number of on-shell resonances and associated visible particles that are needed to get discrete solutions, as compared to considering a single chain.

A significant problem with both the 1-chain and 2-chain approaches is combinatorics.

Advantages and Disadvantages of 1-chain vs. 2-chain approaches.

1-chain:

Less combinatoric ambiguity if you can isolate events in which there are e.g. exactly two leptons, implying that the other side of the event is "simple".

But, must go deeper into the chain to get an equivalent level of constraint (3 visible particles in the chain vs. 2 in minimal cases).

2-chain:

More combinatoric ambiguity (assuming the two chains are the same as in the analyses to be discussed).

But, need not go as deeply into the chain in the minimal case and need fewer events to "solve" in the first solvable situation (2 events vs. 5 events — the 5 events in the 1-chain case, means a high multiplicity of solutions which may more than offset gain on combinatorics).

2 chains — 2 visible particles per chain: (CGHMM)

- **We claim that one can do well at the LHC by taking the more global point of view and using as much information as is available in every event.**

  Consider the chain decay sequence:

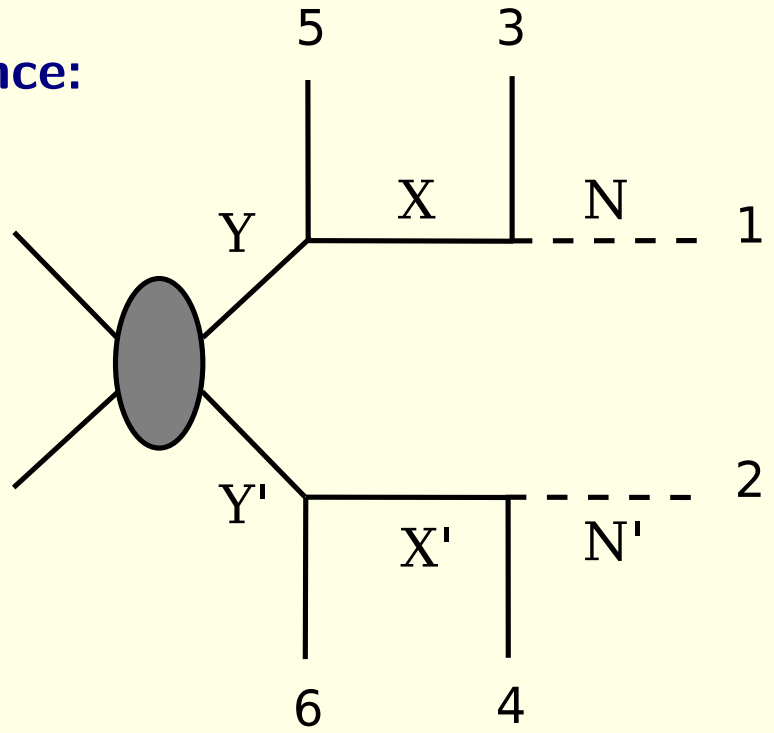

Figure 5: *A typical chain decay topology.*

Note: some cuts to isolate a given topology are required (just as in the previous analyzes) — roughly a ratio of $S/B > 2$ is certain to work.

This topology can be applied to many processes with 4 visible and 2 invisible particles.

We will suppose that $M_Y = M_{Y'}$, $M_X = M_{X'}$, and $M_N = M_{N'}$.

Examples that fit this: $\tilde{\chi}_2^0\tilde{\chi}_2^0 \to l\tilde{l}l\tilde{l} \to ll\tilde{\chi}_1^0 ll\tilde{\chi}_1^0$, $\tilde{q}\tilde{q} \to q\tilde{\chi}_2^0 q\tilde{\chi}_2^0 \to qZ\tilde{\chi}_1^0 qZ\tilde{\chi}_1^0$, and $\tilde{t}\bar{\tilde{t}} \to b\tilde{\chi}^+\bar{b}\tilde{\chi}^- \to bW^+\tilde{\chi}_1^0\bar{b}W^-\tilde{\chi}_1^0$. The first is a subcomponent of the SPS1a chain.

1. In this marginal situation, for each event (with measured visible particle momenta) if we know the 3 masses, then we can solve for the 4-momenta of the N and N' and vice versa.

   The equations are quartic, and so there can be 4, 2 or 0 solutions (with acceptable positive real energies for the N and N'). If not 0, then the event is "solved" for those particular mass choices.

   The code for testing if choices of M_Y, M_X and M_N lead to acceptable p_N and $p_{N'}$ momenta for a given event (specified by the visible particle momenta and $\not{p}_T$, LHE format) is on the Davis WIMPMASS Project website.

2. For each event, we scan through the mass space to see if one or more of

the discrete solutions is acceptable.

Each event then defines a 3-dimensional region in the 3-dimensional mass space that is physically acceptable.

3. As we increase the number of events the 3-dimensional mass region consistent with all events becomes smaller.

   However, in general (and in practice) this region will not shrink to a point.

   Thus, we need additional methods to pick out the correct point in mass space.

- To illustrate our approach, we can consider the explicit example

$$\widetilde{\chi}_2^0\widetilde{\chi}_2^0 \to \ell\widetilde{\ell}\ell\widetilde{\ell} \to \ell\ell\widetilde{\chi}_1^0\ell\ell\widetilde{\chi}_1^0 \quad ,$$
$$i.e. \quad Y = Y' = \widetilde{\chi}_2^0, \quad X = X' = \widetilde{\ell}, \quad N = N' = \widetilde{\chi}_1^0 \, ,$$

which we generate as a subcomponent of

$$\widetilde{q}\widetilde{q} \to q\widetilde{\chi}_2^0 q\widetilde{\chi}_2^0 \to \ldots \to q\ell\ell\widetilde{\chi}_1^0 q\ell\ell\widetilde{\chi}_1^0 \, . \tag{7}$$

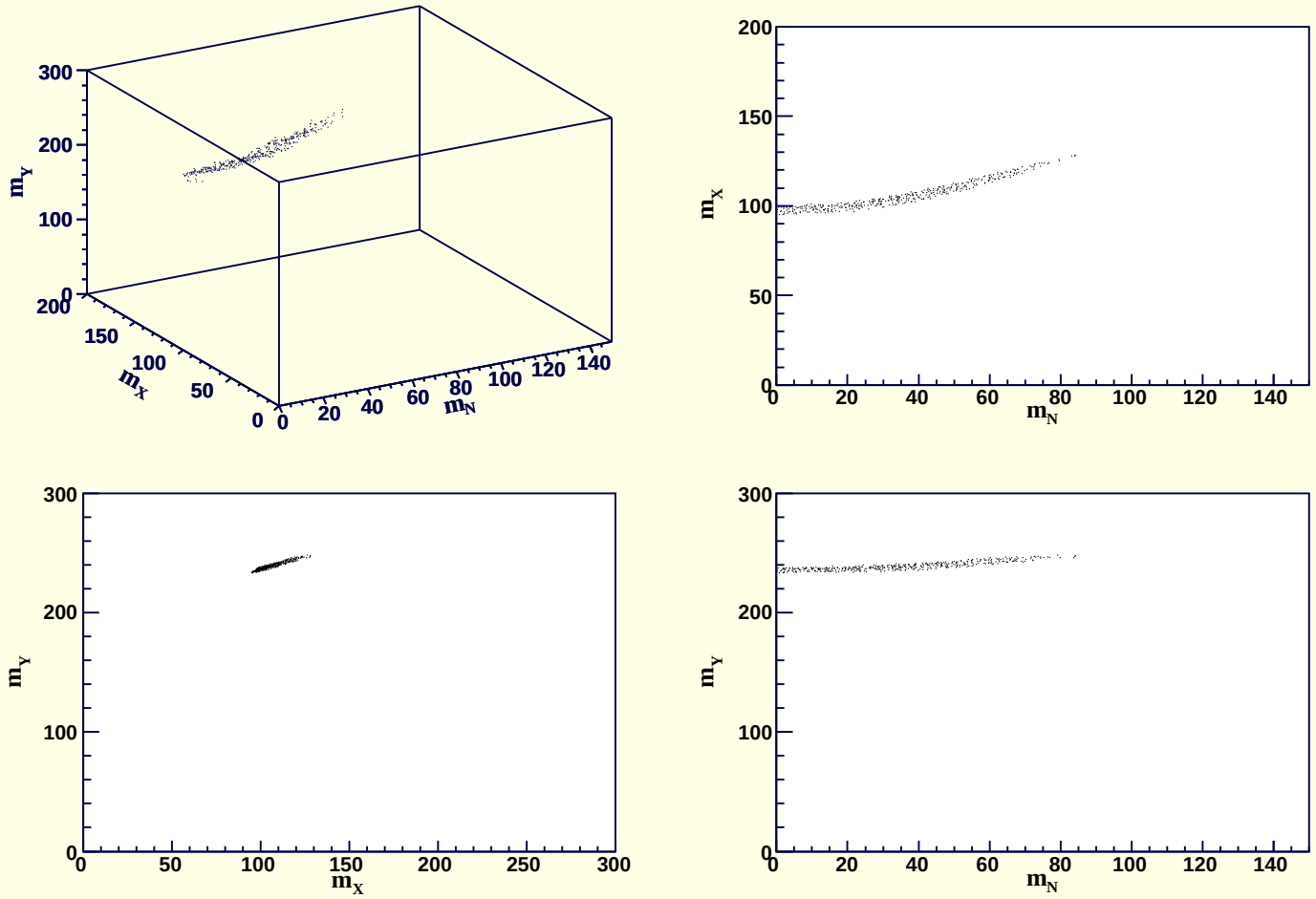

Figure 6: *Mass region (in GeV) that can solve all events.* $\mathbf{500}$ *generated events for* $m_Y = 246.6$ GeV, $m_X = 128.4$ GeV *and* $m_N = 85.3$ GeV, *using correct chain assignments and perfect resolution. Masses from 'Model I', with large* $m_{\tilde{\chi}_2^0}$.

We found that the correct masses lie at the end point of the allowed region.

However, with finite resolutions and combinatorics (which lepton goes where in the two chains), not all events can be solved by the correct mass point.

$\Rightarrow$ The correct mass point will not lie within the intersection region (assuming there is any such region left).

- In the more realistic case, the correct mass choices do not correspond to an endpoint but rather correspond to the choices such that changes in the masses result in the most rapid decline in the number of solved/consistent events.

- One approach to looking for this point of steepest decline in the 3-dimensional mass space employs an iterative approach.

  We vary one mass holding the other two fixed and identify the point at which the number of solved events starts a steep decline as the non-fixed mass is changed.

  A few intermediate one-dimensional fits are shown in Fig. 7, which includes initial and final state radiation, resonance widths, combinatorics and experimental resolutions (as in ATLFAST). Various experimental cuts are made to reduce the SM background to a negligible level.

  We vary M_X, M_Y and M_N in turn (keeping others fixed) and count the number of "solved" events. There is always a peak and sharp edge. Update value of respective mass to peak value.

In the M_N variation step, we record the number of events at the peak. This event number will in general be non-integer.

- **We repeat starting with low value of M_N.**

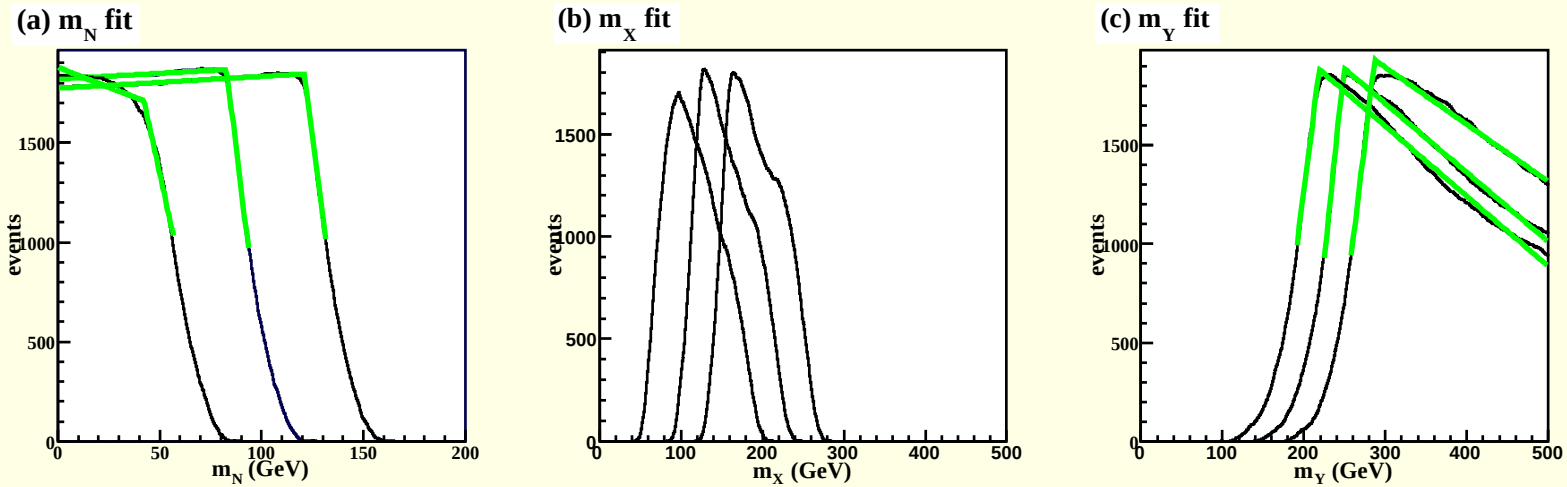

Figure 7: *A few steps showing the migration of the one dimensional fits. The middle curve in each plot corresponds to masses close to the correct values.*

- **The number of events recorded at the M_N peak will in general increase at the beginning and then decrease after some steps, as seen in Fig. 8. Halt the recursive procedure when the number of (fitted) events has sufficiently passed the maximum position.**

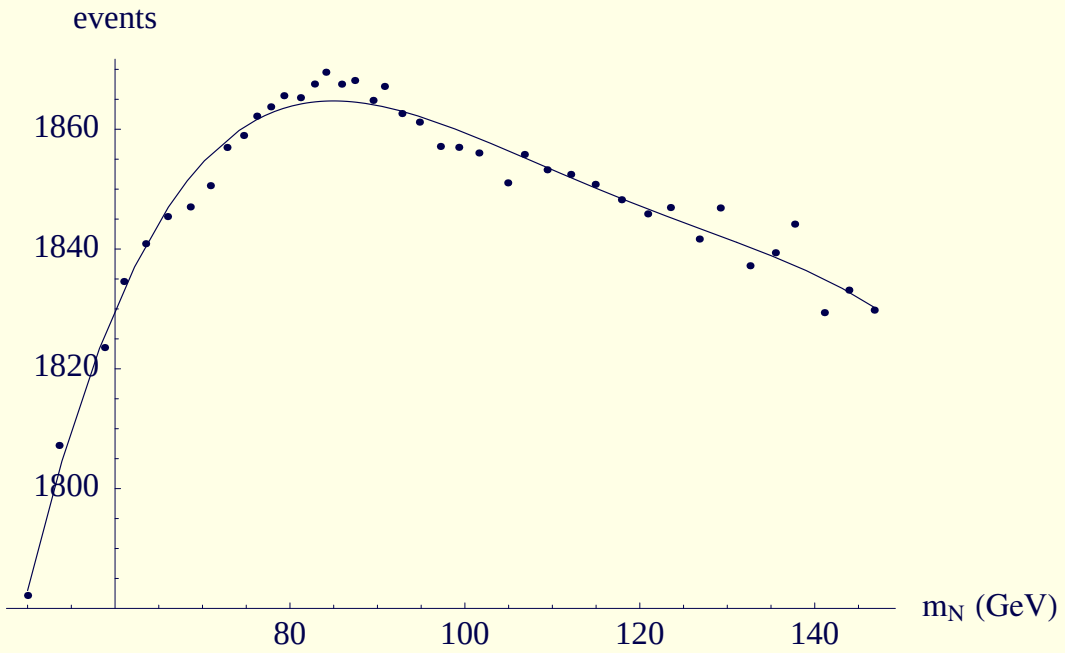

Figure 8: *The final plot for determining m_N. The position of the maximum of the fitted polynomial is taken to be the estimation of m_N..*

Remarkably, the point at which the turnover occurs gives M_N to good accuracy.

- **Fit Fig. 8 to a (quartic) polynomial and take the position where the polynomial is maximum as the estimated M_N.**

- **Keep M_N fixed at the above value and do a few one-dimensional fits**

for M_Y and M_X until they are stabilized. Take the final values as the estimates for M_Y and M_X.

A deeper understanding of our procedure can be gained by examining the graphical representation of the steps taken in the (M_Y, M_N) plane shown in Fig. 9.

There, we display contours of the number of (fitted) events after maximizing over possible M_X choices.

There is a 'cliff' of falloff in the number of solved events beyond about 1825 events. It is the location where this cliff is steepest that is close to the input masses, which are indicated by the (red) star.

The mass obtained by our recursive fitting procedure is indicated by the (blue) cross.

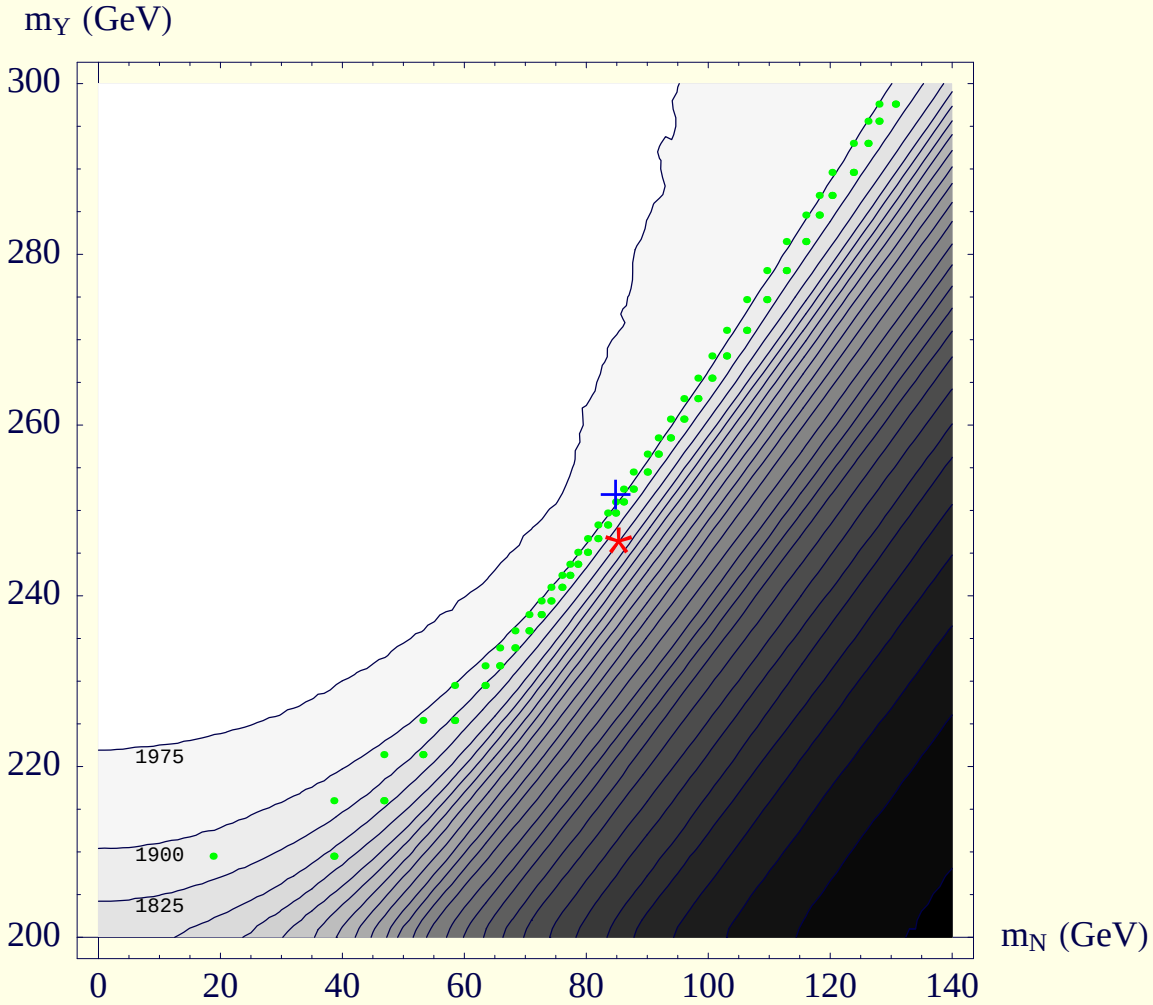

Figure 9: *"Model 1" example. Contours for the number of solved events in the $M_N \sim M_Y$ plane with 2000 events. The number of events is the maximum value obtained after varying M_X. Contours are plotted at intervals of 75 events, beginning with a maximum value of 1975. The green dots correspond to a set of one-dimensional fits. The ⋆ shows the input masses and the + shows our fitted masses.*

- **Error evaluation:**

Must adopt an 'experimental' approach for such an empirical procedure:

Generate 10 different $90\ \mathrm{fb}^{-1}$ data Model 1 samples and apply the procedure to each sample. For this study we used ATLFAST.

Estimate the errors of our method by examining the statistical variations of the 10 samples, which yields

$$M_Y = 252.2 \pm 4.3\text{GeV}, \quad M_X = 130.4 \pm 4.3\text{GeV}, \quad M_N = 86.2 \pm 4.3\text{GeV}. \tag{8}$$

The statistical variations for the mass differences are much smaller:

$$\Delta M_{YX} = 119.8 \pm 1.0\text{GeV}, \quad \Delta M_{XN} = 46.4 \pm 0.7\text{GeV}. \tag{9}$$

Compared with the correct values $\mathcal{M}_A = \{246.6, 128.4, 85.3\}$, we observe small biases in the mass determination, which means that our method has some "systematic errors".

However, these systematic errors are determined from Monte Carlo (purely

kinematic level) once we fix the experimental resolutions, the kinematic cuts and the fit procedure.

Therefore, they can be easily corrected for, which leaves us errors for the absolute mass scale of $\sim few$ GeV and for the mass differences of ~ 1 GeV which will decrease further after adding in $2e2\mu$ and $4e$ final states.

The SPS1a Point

- It is desirable to compare directly to the results obtained by others for the SPS1a SUSY parameter point.

- For the usual SPS1a mSUGRA inputs the masses for $Y = \widetilde{\chi}_2^0$, $X = \widetilde{\mu}_R$ and $N = \widetilde{\chi}_1^0$ (from ISAJET 7.75) are

$$m_{\widetilde{\chi}_2^0} = 180.3 \text{ GeV}, \quad m_{\widetilde{\mu}_R} = 142.5 \text{ GeV}, \quad m_{\widetilde{\chi}_1^0} = 97.4 \text{ GeV} \qquad (10)$$

- We perform the analysis using the same $4\mu\widetilde{\chi}_1^0\widetilde{\chi}_1^0$ final state that we have been considering.

- This is a more difficult case than Point I considered earlier due to the fact that the dominant decay of the $\widetilde{\chi}_2^0$ is $\widetilde{\chi}_2^0 \to \tau\widetilde{\tau}_1$.

  The branching ratio for $\widetilde{\chi}_2^0 \to \mu\widetilde{\mu}_R$ is such as to leave only about 1200 events (using ATLFAST) in the $4\mu\widetilde{\chi}_1^0\widetilde{\chi}_1^0$ final state after $L = 300\ \mathrm{fb}^{-1}$ of accumulated luminosity.

- Cuts reduce the number of events further to ~ 425.

- After including combinatorics and resolution we obtain:

$$M_Y = 188 \pm 12\ \mathrm{GeV}\,, \quad M_X = 151 \pm 14\ \mathrm{GeV}\,, \quad M_N = 100 \pm 13\ \mathrm{GeV}\,. \tag{11}$$

  Errors are determined by generating many such plots for different samples of ~ 425 events (the exact number changes depending upon event details).

  Errors will come down to about $\pm 5\ \mathrm{GeV}$ after including $2e2\mu$ and $4e$ final states, making our results comparable to the ATLAS LHC edge results.

  Biases can be removed using Monte Carlo.

Two interesting variations: CH

Use the $M_{T2}^{max}(\mu_N)$ curve, possibly along with dilepton edge location, plus the "solution" procedure.

1. **With dilepton edge:**

   (a) Follow the $M_{T2}^{max}(\mu_N)$ curve which gives $\mu_Y = M_{T2}^{max}(\mu_N)$ given μ_N.
   (b) Use the dilepton edge constraint:

$$M_{\ell\ell}^2|_{edge} = \frac{(M_Y^2 - M_X^2)(M_X^2 - M_N^2)}{M_X^2} \tag{12}$$

   to establish value of μ_X (two-fold ambiguity) for the values of μ_N and $\mu_Y(\mu_N)$ defined by M_{T2}^{max} curve.
   (c) Count the number of consistent "solved" events as you move along the M_{T2}^{max} curve varying μ_N.
   (d) Strong peak is observed at value of μ_N when $\mu_N = M_N$.

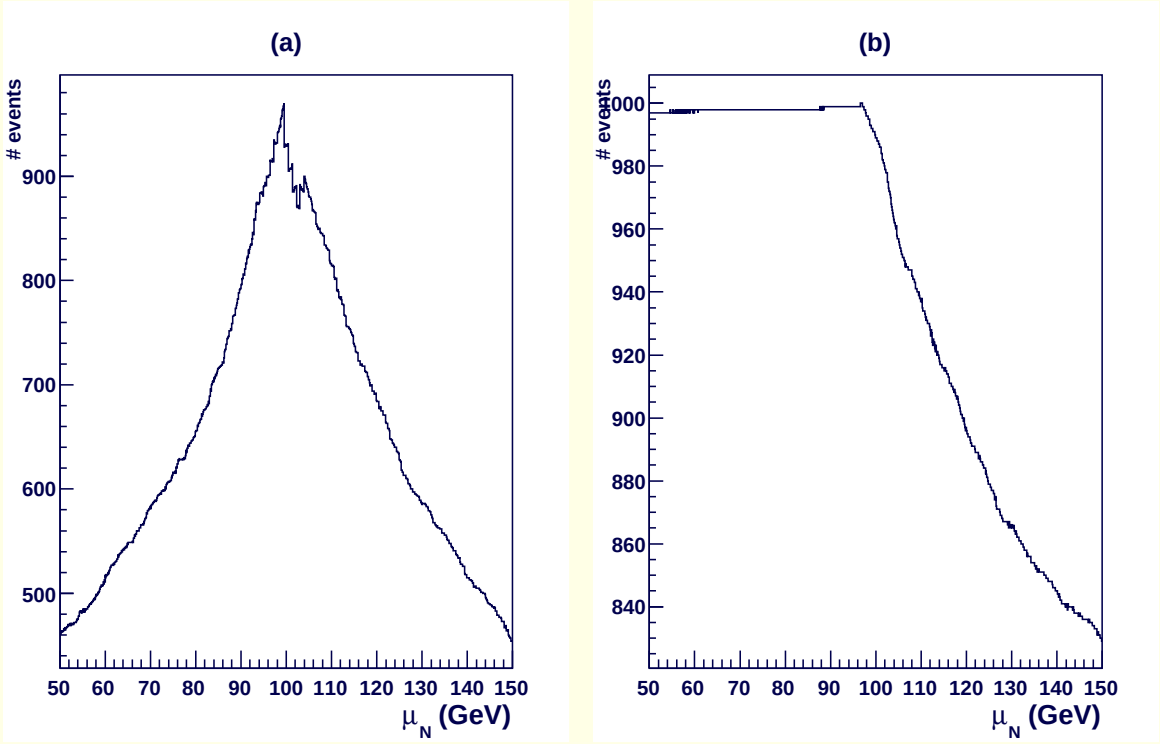

Figure 10: *M_N determination following $M_{T2}^{max}(\mu_Y)$ curve: left=using dilepton edge; right=without dilepton edge information. No smearing, combinatorics.*

2. Without dilepton edge:

(a) Fix $\mu_Y(\mu_N)$ for each trial μ_N using M_{T2}^{max} curve.
(b) *Vary* μ_X and look for maximum in the number of consistent "solved" events for given μ_N.
(c) Plot this maximum number as a function of μ_N.
(d) Correct value of μ_N is located at the maximum of the former maximum.

These plots are before resolution and combinatorics — under study.

2 chains: 3 visible particles per chain: CEGHM, CGHM

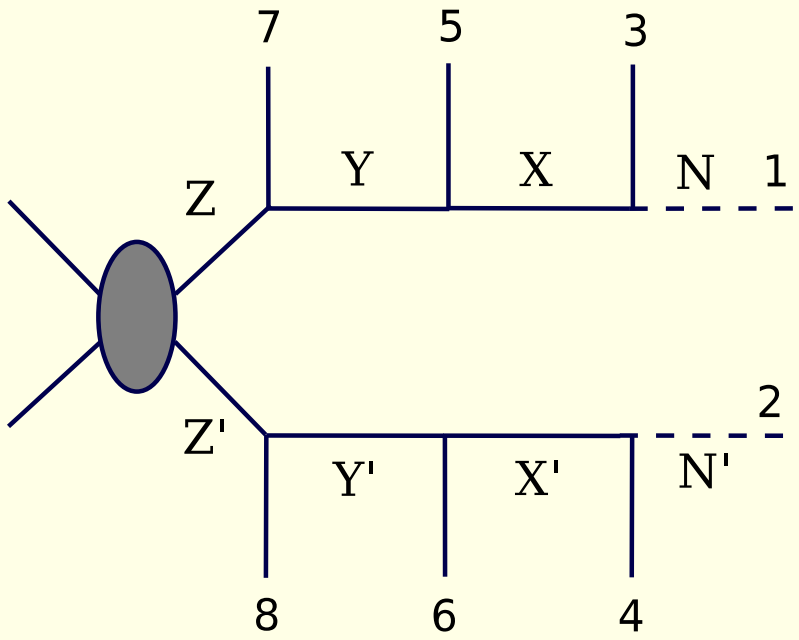

Figure 11: The 3-visible per chain topology.

- **Recall from the counting section that to solve requires just $n = 2$ events.**

  Altogether, using measured visible particle momenta and $\not{p}_T$ for 2 events, one finds 16 unknowns and 16 equations. The system can be solved numerically and we obtain discrete solutions for p_1, p_2, q_1, q_2 and thus the masses M_N, M_X, M_Y, and M_Z.

Note that the equations always have 8 complex solutions, but we will keep only the real and positive ones which we henceforth call "solutions".

The code for getting the mass solutions for any given pair of events is found on the Davis WIMPMASS Project web site.

Of course, the wrong solutions are different from pair to pair, but the correct solution is common.

It is easy to get lots of pairs of events.

We focus on the SPS1a decay chain $\widetilde{q} \to q\widetilde{\chi}_2^0 \to q\mu\widetilde{\mu}_R \to \widetilde{\chi}_1^0 q\mu\mu$ with SPS1a masses $m_{\widetilde{u},\widetilde{d}} = 564.8\ \mathrm{GeV}, 570.8\ \mathrm{GeV}$, $m_{\widetilde{\chi}_2^0} = 180.3\ \mathrm{GeV}$, $m_{\widetilde{\mu}_R} = 142.5\ \mathrm{GeV}$ and $m_{\widetilde{\chi}_1^0} = 97.4\ \mathrm{GeV}$.

We first consider the ideal case: no background events, all visible momenta measured exactly, all intermediate particles on-shell and each visible particle associated with the correct decay chain and position in the decay chain.

We also restrict the squarks to be up-type only.

In this case, we can solve for the masses exactly by pairing any two events.

The only complication comes from there being 8 complex solutions for the system of equations, of which more than one can be real and positive.

The mass distributions for the ideal case with 100 events are shown in Fig. 13.

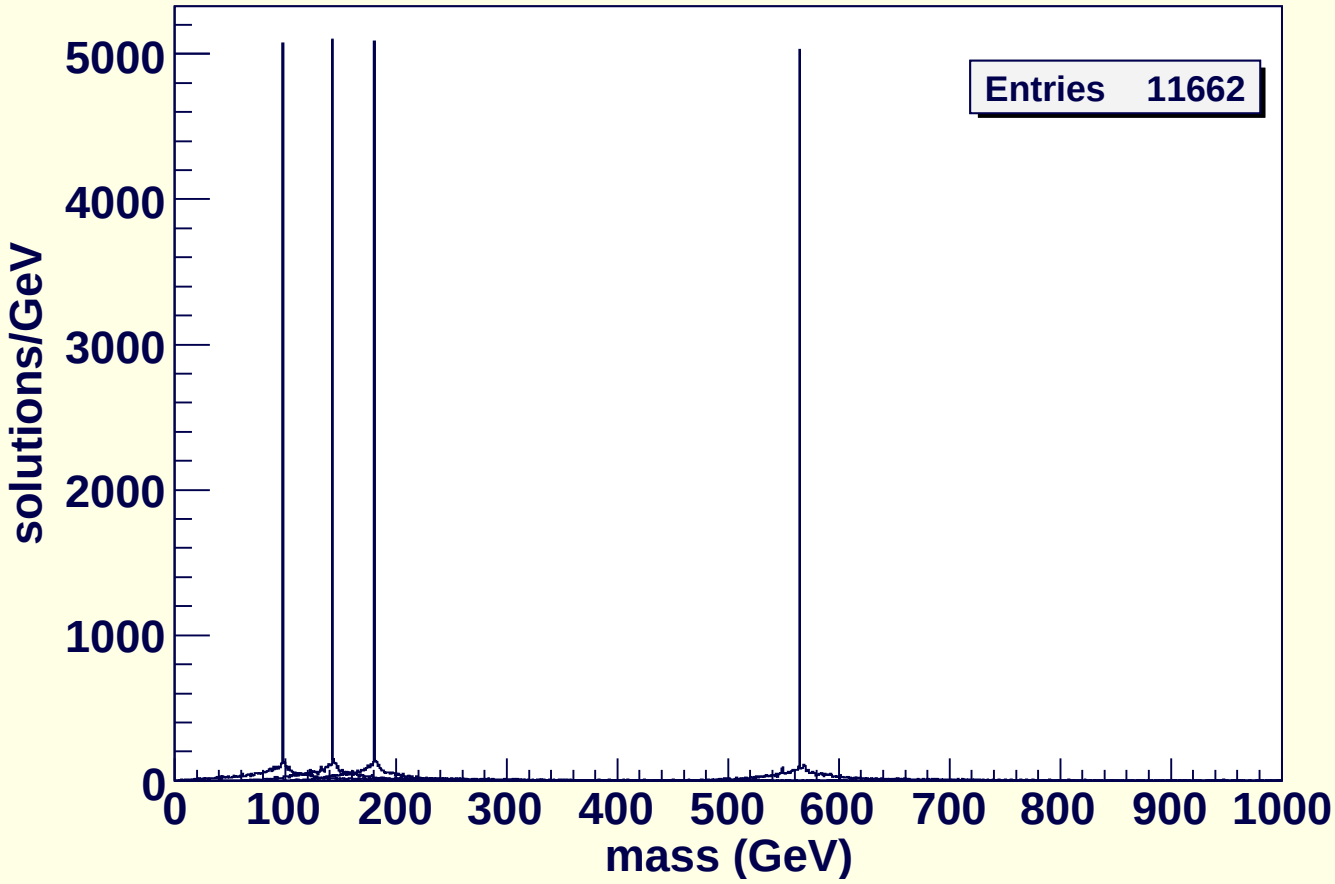

Figure 12: We plot the number of mass solutions (in 1 GeV bins — the same binning is used for the other plots) vs. mass in the ideal case. All possible pairs for 100 events are included.

As expected, we observe δ-function-like mass peaks on top of small backgrounds coming from wrong solutions. On average, there are about 2

solutions per pair of events.

The δ-functions in the mass distributions arise only when exactly correct momenta are input into the equations we solve.

To be experimentally realistic, we now include the following.

1. **Wrong combinations.**

For a given event a "combination" is a particular assignment of the jets and leptons to the external legs of Fig. 12. For each event, there is only one correct combination (excluding $1357 \leftrightarrow 2468$ symmetry).

Assuming that we can identify the two jets that correspond to the two quarks, we have 8 (16) possible combinations for the $2\mu 2e$ (4μ or $4e$) channel.

The total number of combinations for a pair of events is the product of the two, *i.e.* 64, 128 or 256.

Adding the wrong combination pairings for the ideal case yields the mass

distributions of Fig. 14.

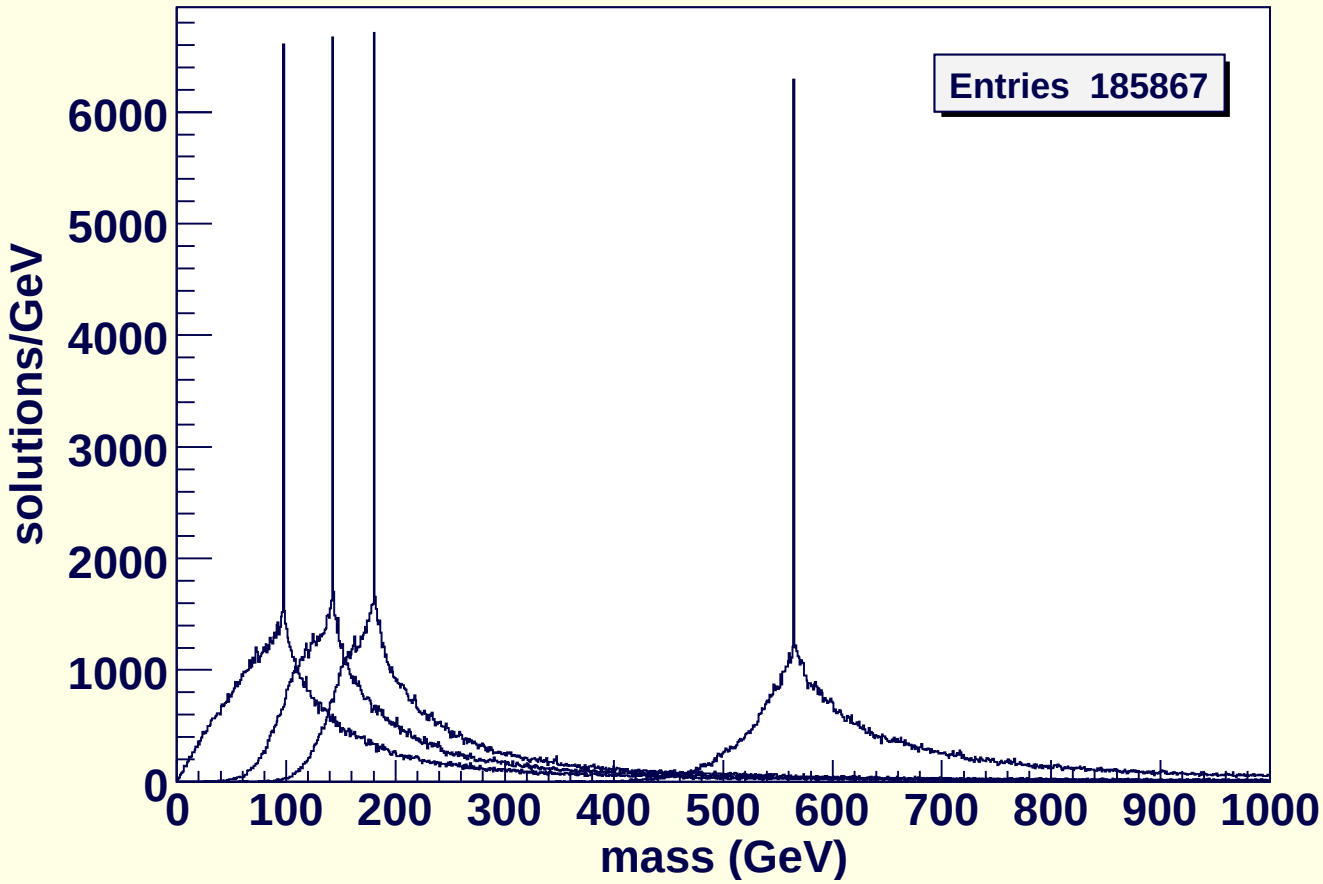

Figure 13: Number of mass solutions versus mass after including all combination pairings for 100 events.

Compared to Fig. 13, there are 16 times more (wrong) solutions, but the δ-function-like mass peaks remain evident.

2. **Finite widths.**

3. **Mass splitting between flavors.**

4. **Initial/final state radiation.** These two types of radiation not only smear the visible particles' momenta, but also provide a source for extra jets in the events. We will apply a p_T cut to get rid of soft jets.

5. **Extra hard particles in the signal events.**

6. **Background events.** The SM backgrounds are negligible for this signal in SPS1a. Backgrounds from other SUSY processes are very small after our cuts.

7. **Experimental resolutions.** In order to estimate this experimental effect at the LHC, we process all events with PGS (vs. ATLFAST of shorter paper). PGS yields fewer surviving events (more stringent lepton isolation cuts) implying larger errors than we found for ATLFAST.

For a data sample with $300\ \mathrm{fb}^{-1}$ integrated luminosity, there are about 620 (vs. 1050 using ATLFAST) events left after basic signal isolation cuts, out of which about 420 are signal events. After taking all possible pairs for all possible combinations and solving for the masses, we obtain the mass distributions in Fig. 15.

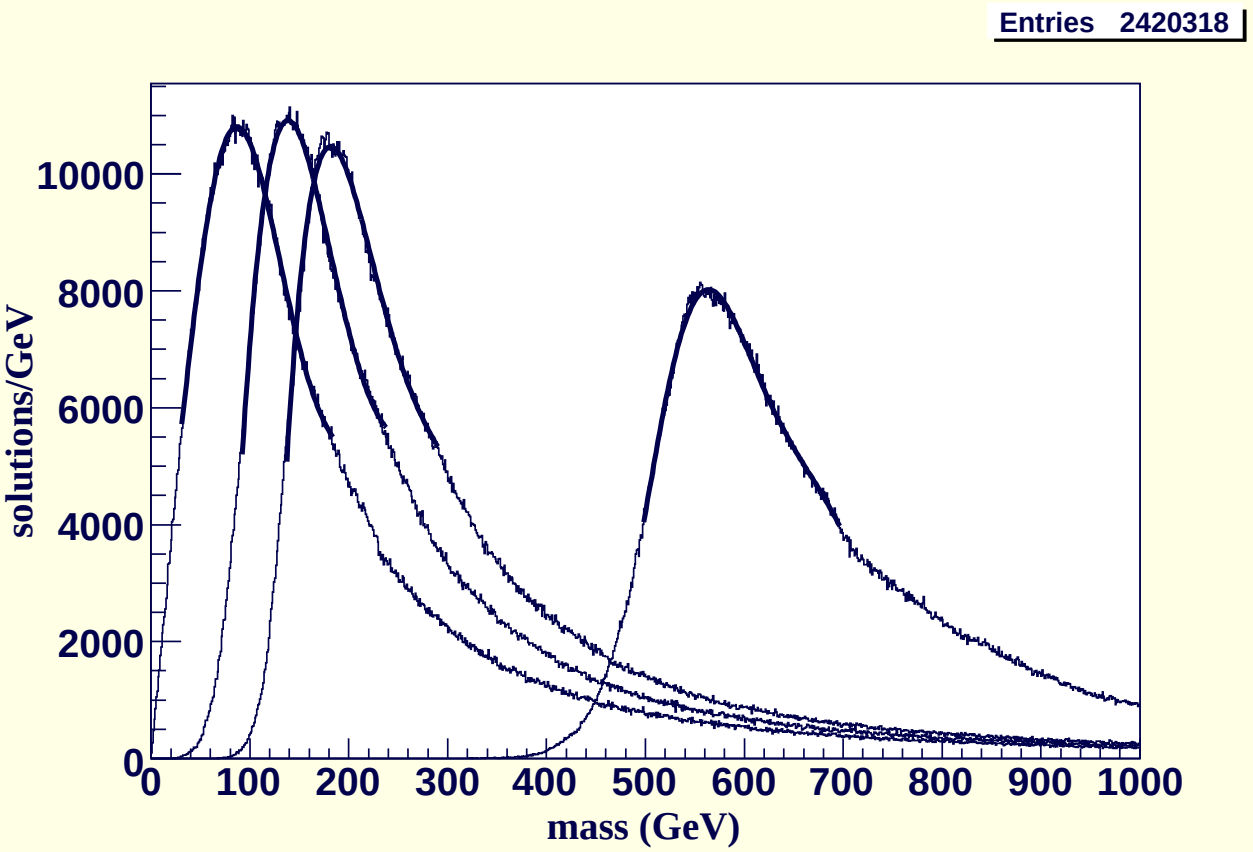

Figure 14: Mass solutions with all effects 1 – 7 included and after cuts I – III for the SPS1a SUSY model and $L = 300\ \mathrm{fb}^{-1}$.

Fitting each distribution using a sum of a Gaussian plus a (single) quadratic polynomial and taking the maximum positions of the fitted peaks as the estimated masses yields $78.4, 134.2, 181.5, 553.9$ GeV. Averaging over 20 different data samples, we find

$$M_N = 76.7 \pm 2 \text{ GeV}, \quad M_X = 134.6 \pm 2.2 \text{ GeV},$$
$$M_Y = 178.9 \pm 3.8 \text{ GeV}, \quad M_Z = 561.6 \pm 5.4 \text{ GeV}.$$

The statistical uncertainties are very small (and smaller than ATLAS results for this same chain, despite using PGS, which gives fewer final events than ATLFAST) but there exist biases, especially for the two light masses.

In practice, we can always correct the biases by comparing real data with Monte Carlo.

Nevertheless, it is perhaps more satisfying to reduce the biases as much as possible using data only.

In some cases, the biases can be very large and it is essential to reduce them before comparing with Monte Carlo.

The combinatorial background is an especially important source of bias since it yields peaked mass distributions that are not symmetrically distributed

around the true masses, as can be seen from Fig. 14.

This will introduce biases that survive even after smearing. Therefore, we developed a procedure for reducing wrong solutions (param. f_{cut}).

Next, we found a procedure for increasing the weight of the correct solution.

We also found it useful to keep only those solutions for which *all three* mass differences fall within certain mass difference windows.

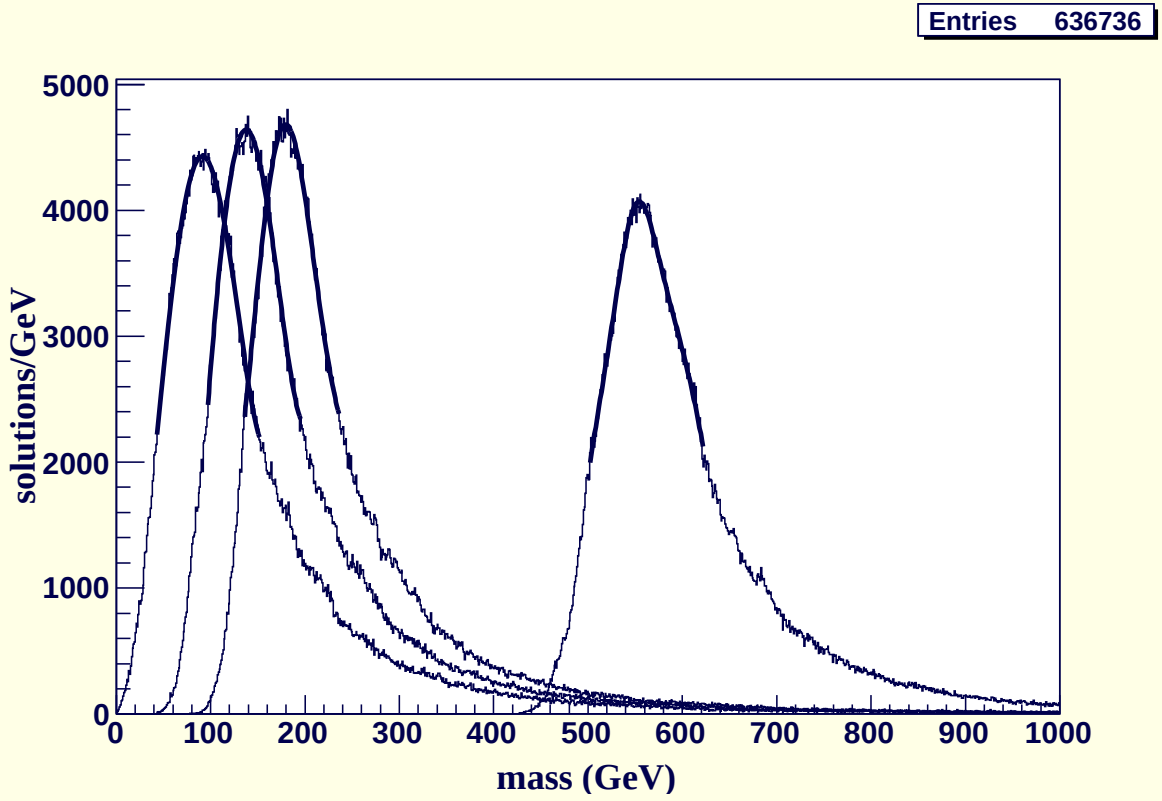

Figure 15: Final mass distributions after the bias-reduction procedure for the SPS1a SUSY model and $L = 300$ fb^{-1}.

Repeating the procedure for 20 data sets, we find

$$M_N = 93.8 \pm 3.9 \text{ GeV}, \quad M_X = 138.4 \pm 4.5 \text{ GeV},$$
$$M_Y = 178.7 \pm 4.6 \text{ GeV}, \quad M_Z = 559.5 \pm 5.4 \text{ GeV}.$$

(compared to somewhat larger ATLAS edge errors despite PGS) vs. inputs

$$M_N = 97.4 \text{ GeV}, \quad M_X = 142.5,$$
$$M_Y = 180.3 \text{ GeV}, \quad M_Z = 564.8, 570.8 \text{ GeV}.$$

The biases are reduced at the cost of (slightly) increased statistical errors.

We reemphasize that the remaining biases in the above mass determinations can be removed by finding those input masses that yield the observed output masses (in fact mass distribution plots) after processing Monte Carlo generated data through our procedures. In this way, very accurate central mass values are obtained with the indicated statistical errors.

Further checks and tests

- We have applied our method to other mass points to show its reliability.

- We have demonstrated that the results are independent of spin by comparing SUSY to a UED model with exactly same masses.

- We have demonstrated that extracted masses are very robust as available integrated L declines.

- We have demonstrated that errors worsen rather slowly as (artificial in case of SPS1a) background is introduced, especially if we employ a relatively mild dilepton edge cut.

- The dilepton edge cut procedure described below also essentially eliminates all biases with only a small sacrifice in accuracy.

The DiLepton Edge Cut

- Ignoring resolution smearing, kinematics predicts that correct combinations should have

$$(M_{\ell\ell}^{\rm edge})^2 = \frac{(M_{Y0}^2 - M_{X0}^2)(M_{X0}^2 - M_{N0}^2)}{M_{X0}^2}, \qquad (13)$$

where M_{Y0}, M_{X0} and M_{N0} are the input masses.

Indeed a sharp dilepton edge is visible in the Monte Carlo data even after allowing for combinatorics, smearing, etc.

- Before employing the bias reduction procedure, we apply a cut on the M_Y, M_X, M_N values obtained for a given solution of

$$\left| \sqrt{(M_Y^2 - M_X^2)(M_X^2 - M_N^2)/M_X^2} - M_{\ell\ell}^{\rm edge} \right| < 20 \text{ GeV}, \qquad (14)$$

where we have purposely employed a rather loose cut so as to not lose statistics and to take into account smearing of the input X, Y, N masses that will be present even for a correct combination, as well as the small error associated with determining the edge location experimentally.

- The resulting mass distributions are now essentially unbiased and very sharp.

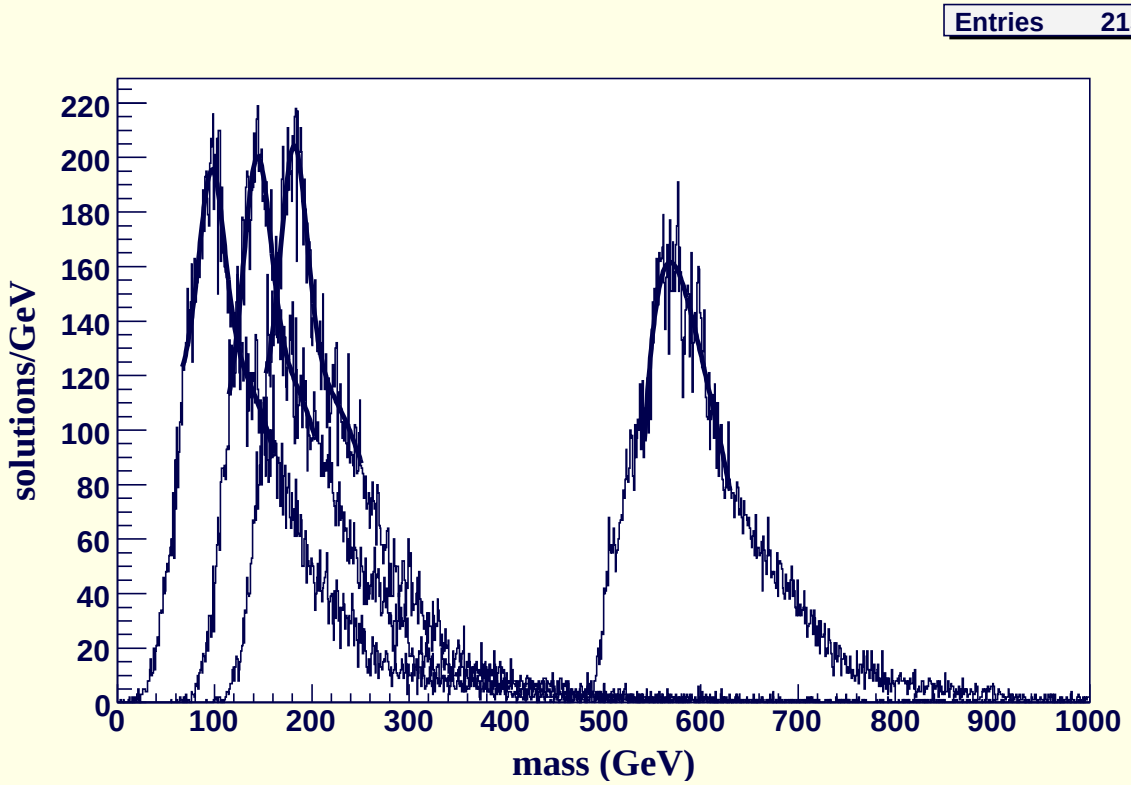

Figure 16: Final mass distributions after dilepton edge cut and the bias-reduction procedure (using $f_{cut} = 0.75$) for the SPS1a SUSY model and $L = 300$ fb^{-1}.

Bias removal occurs because many of the wrong solutions have been eliminated.

For example, after the dilepton edge cut and after employing the bias-reduction procedure using $f_{cut} = 0.75$, about 160 events are retained on average and the average number of solutions for the remaining pairs formed from these surviving events is only about 1.2.

	with dilepton edge cut				without dilepton edge cut			
f_{cut}	0.60	0.65	0.70	0.75	0.60	0.65	0.70	0.75
m_N	93.0 ± 3.7	96.1 ± 3.9	97.5 ± 4.3	97.9 ± 4.9	85.6 ± 2.3	88.1 ± 3.5	90.7 ± 3.8	93.8 ± 3.9
m_X	138.9 ± 3.9	141.4 ± 4.6	143.7 ± 4.6	144.3 ± 4.0	131.5 ± 2.7	133.9 ± 3.6	135.9 ± 4.3	138.4 ± 4.5
m_Y	176.5 ± 3.8	178.8 ± 4.6	180.8 ± 5.1	181.5 ± 5.3	172.8 ± 2.8	174.8 ± 3.8	176.6 ± 4.4	178.7 ± 4.6
m_Z	557.8 ± 4.4	559.9 ± 4.5	563.2 ± 5.0	565.6 ± 6.2	555.8 ± 5.2	557.2 ± 5.5	557.8 ± 5.1	559.5 ± 5.4

Table 1: Peak locations for various values of f_{cut} (a bias reduction parameter) with and without the dilepton edge cut. Errors were determined using 20 distinct data sets.

- **Errors for the peak mass values are, of course, slightly larger when a dilepton edge cut is imposed,**

  $\Rightarrow$ ultimately the best mass determinations may be those obtained using Monte Carlo determination of the bias corrections that should be applied to mass peak values obtained without the dilepton edge cut.

  Nonetheless, doing the analysis with a dilepton edge cut will provide a very important cross check of the bias determination.

- **Dilepton edge cut totally kills $\widetilde{\tau}$ background (primary $\widetilde{\chi}_2^0$ decay mode).**

Conclusions

- There are now a lot of techniques for mass determination in the presence of two chains, each ending in an invisible particle.

- Not sure who is winning, but the Davis techniques for mapping from event space to mass space are certainly very good.

- Especially useful seems to be combining the above mapping with a dilepton edge cut. One should explore throwing M_{T2}^{max} into the mix.

- Don't forget that we must understand how to single out a single topology ($i.e.$ suppress others adequately) in the case that there are many new physics topologies.

  If this cannot be done, then we must learn how to work with multiple topologies. We believe our techniques can be generalized to such a situation.

- Try out the Davis WIMPMASS Project website, under HEFTI/Projects.